Bio-ferroelectric properties of glycine crystals

Pengfei Hu,[ab] Shunbo Hu,[bc] Yundi Huang,[ab] Yongxue Tao,[b] Jeffrey R. Reimers,[bc] Yongle Li,*[b] Alessandro Stroppa,*[bd] and Wei Ren*[be]

[a] Department of Chemistry, Shanghai University, Shanghai 200444, China.

[b] Department of Physics and International Center of Quantum and Molecular Structures, Shanghai University, Shanghai 200444, China.

[c] School of Mathematical and Physical Sciences, University of Technology Sydney, NSW 2007, Australia

[d] CNR-SPIN, Via Vetoio, L'Aquila 67100, Italy

[e] Materials Genome Institute, Shanghai Key Laboratory of High Temperature Superconductors, Shanghai University, Shanghai 200444, China

*Emails: alessandro.stroppa@spin.cn.it, yongleli@shu.edu.cn; renwei@shu.edu.cn

Abstract

Biological ferroelectric materials have great potential in biosensing, disease diagnosis and treatment. Using density functional theory, we calculate the polarizations of two phases of glycine crystals, namely the β- and γ-phases, showing them to be comparable to those of conventional inorganic ferroelectrics. Further, molecular dynamics simulations embodying polarized crystal charges predict Curie temperature of γ-glycine to be 630 K, with a required coercive field to switch crystalline polarization states of 1 V nm^{-1}, consistent with experimental evidence. This sheds light on the microscopic mechanism of electric dipole ordering in biomaterials, something useful in the materials design of new bio-ferroelectrics.

Introduction

The study of ferroelectricity and piezoelectricity in bio-systems provides an exciting combination of physics and biology,[1] starting with the discovery of piezoelectric properties in wood by Fukada in the 1950s.[2] Advanced experimental techniques have allowed the discovery of piezoelectric and ferroelectric properties of many other biomaterials, including bones, aortic walls, nails, teeth, seashells, and peptide nanotubes.[3-9] However, general principles depicting mechanisms for ferroelectric switching in biomaterials are not available, perhaps owing to the complexity of bio-systems. An example of an identified principle comes from the recent study of Hu *et al.* that discussed switchable dipole long-range ordering in an important biomaterial, hydroxyapatite, using firsxt-principle methods.[10]

Recently, it was demonstarted that a basic component of biological structure, namely glycine, presented nanoscale ferroelectricity.[11] Glycine is one of the simplest and smallest biological molecules. It therefore presents a starting point for the design of functional materials as it can be synthetically modified to optimize properties.

Interestingly, its crystals have been shown to be ferroelectric.[11] As it is a molecule sometimes taken to represent the symbol of life,[12] it also represents a paradigm for the understanding of bio-ferroelectricity. Much is known about its crystal phases,[13] but little is known concerning how useful its bio-ferroelectric properties may be in potential applications.

Glycine mainly exists in either its α-, β- or γ- phases under ambient conditions.[14] Alternative δ-, ε- and ζ- phases are known but are metastable, being observable only under special conditions.[15-16] The α-glycine (symmetry group $P2_1/m$) has an antiparallel layered hydrogen bond network, first reported by Albrecht and Corey,[14] that can remain stable at room temperature. The β-glycine (symmetry group $P2_1$), first reported by Iitaka and Bernal,[17] has a parallel layered hydrogen-bond network. Under ambient condition, it usually transforms into either the α- or γ-phases, giving rise to potential practical applications. γ-glycine (forming in either symmetry group $P3_1$ or $P3_2$) is the most stable phase, and was first obtained by Iitaka.[18] It has a helical hydrogen bonding network, a feature not found in the other two phases. The three dominant phases of glycine crystals have relative stability γ > α > β. Another feature of technological relevance is that phases can interconvert under certain conditions, including in response to humidity changes,[19] with only the γ-phase remaining unconditionally stable in moist air.[13] A phase transition from β-glycine to either α- or γ-glycine is automatically obtained when the humidity increases. Similarly, the α-phase can also change to the γ-phase at high humidity. When the temperature increases above 443 K, the γ-phase can change to the α-phase, but this transition temperature can be modulated.[19-20] The polymorphism observed between the known phases of glycine is summarized in the Figure 1. Since $P2_1/m$ is centrosymmetric, there is no net polarization within the α-phase, while the polar phases, β- and γ-, have polarization along the b-axis and c-axis, respectively.

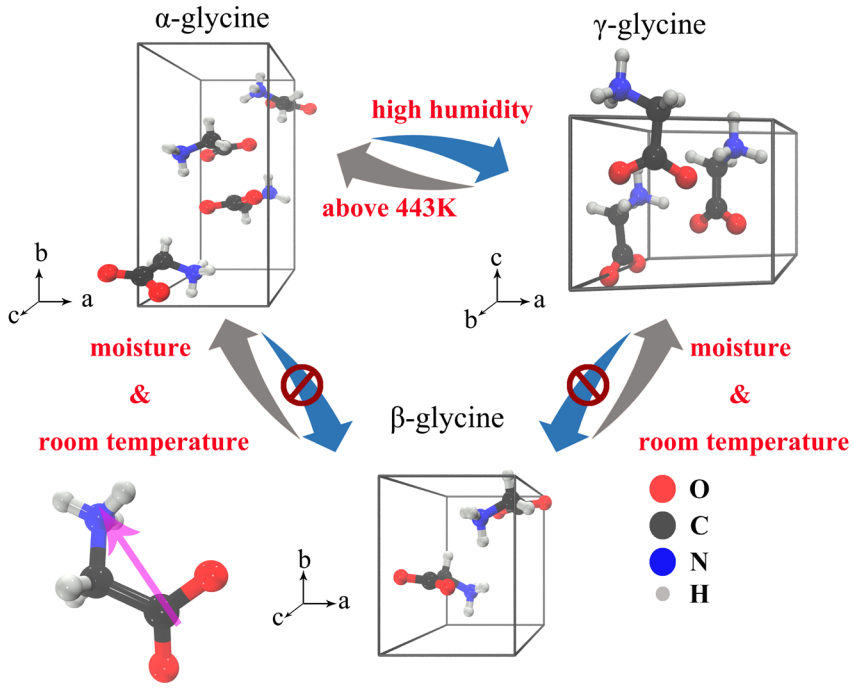

Figure 1. Ball-and-stick models of glycine phase conversion. The purple arrow represents the molecular dipole moment. Since the α-phase is centrosymmetric, there is no net polarization for this phase, while polarizations arising in β-glycine and γ-glycine are directed along the b-axis and c-axis, respectively.

Glycine crystals have been previously simulated,[21] but issues such as the potential usefulness of its bio-ferroelectricity were not addressed. In this work, we perform first-principle density functional theory (DFT) molecular dynamics (MD) simulations, elucidating key ferroelectric properties of glycine. In particular, we consider the β-(monoclinic, $P2_1$) and γ-phases (triangular, $P3_1$ and $P3_2$) phases using Modern Polarization Theory (MPT).[22] Furthermore, we employ MD simulations embodying a new charge method to study polarization switching of the γ-phase. We simulate the hysteresis loop and the γ-phase transition as a function of the temperature, reproducing the reduction of the polarization that occurs as the paraelectric phase is approached.

Methods

The structure used to calculate the ferroelectric polarization of glycine is derived from the observed crystal structure[13, 23-24] obtained from the Cambridge Crystallographic Data Centre (CCDC).[25] The structure of α-glycine refined at T=294 K (symmetry group $P2_1/m$, Z =4) is centrosymmetric, with lattice parameters of: a = 5.105 Å, b = 11.972 Å and c = 5.463 Å. Alternatively, the β-glycine and γ-glycine crystals are both polar. The lattice parameters for β-glycine (symmetry group $P2_1$, Z =2) are: a = 5.093 Å, b = 6.272 Å and c = 5.385 Å. For γ-glycine in symmetry group $P3_1$, Z =3, the lattice parameters are: a = b = 7.038 Å and c =5.481 Å, while alternatively for symmetry group $P3_2$, Z =3 they are: a = b = 7.037 Å and c =5.481 Å.

All first-principles electronic-structure calculations were performed using the Vienna ab-initio Simulation Package (VASP),[26] using the projector-augmented-wave (PAW) method to treat the interactoions between the valence-electrons and their inner core.[27-28] Most calculations were performed using the Perdew-Burke-Ernzerhof (PBE) exchange correlation functional, but in test studies the LDA,[29] PBE (including D2 and D3 correction),[28, 30-31] PBEsol (PBE for solids),[32] SCAN[33] and the latest SCAN+rvv10 functionals[34] are also used. The energy cutoff is set to 400 eV. The Brillouin zone was sampled with Monkhorst–Pack k-points mesh of $6 \times 6 \times 6$ for β-glycine, while $6 \times 4 \times 6$ were used for the γ-glycine calculations. The convergence of the Hellmann-Feynman force and the total energy is set to 0.01 eVÅ^{-1} and 10^{-6} eV, respectively. VESTA is used to draw crystal structure graphics.[35]

Based on the first-principles calculations, MPT is used to deduce crystal polarizations. This approach expresses ferroelectric polarization as $\Delta P = \Delta P_{\text{ion}} + \Delta P_{\text{ele}}$. Here, the electronic contribution (ΔP_{ele}) is evaluated by the Berry phase approach. This method correctly accounts for quantum electronic effects associated with moving charges across unit-cell boundaries.[36-37] We evaluated ΔP_{ele} simply using VASP. For ΔP_{ion}, however, the MPT method relies on the conception of some paraelectric phase (PE) that can be continuously morphed into the ferroelectric phase (FE) of interest. We follow the detailed description of how to construct a proper PE reference state described recently by Hu et al..[38] A dimensionless parameter λ is introduced to describe the path. It represents a correlated atomic displacement field whose ampli-

tude is normalized to 1. Along the path, λ varies from 0 for the case of the reference centrosymmetric structure to λ= 1 for the ferroelectric structure. A linear interpolation of the atomic positions between the two reference structures is employed. The use of such a path allows smooth evolution of polarization to be ensured, guaranteeing that no quantum of polarization has been erroneously included in the final result.

In this work, two potential ferroelectric phases of glycine crystals are considered: the β-phase and γ-phase. The reference phases for β-glycine and γ-glycine are constructed using the tools Bilbao Crystallographic Server, such as PSEUDO[39] and AMPLIMODES.[40-41]

In a second part of the study, we use molecular dynamic (MD) simulations based on the generalized AMBER[42] force field (GAFF). Especially, the partial charges for the atoms in zwitterionic forms of glycine were derived using the scheme of a recently developed polarized protein-specific charge (PPC).[43-44] The method is modified slightly to properly treat periodic crystal models, applying the polarized crystal charge (PCC) model.[REF] During the MD simulations, a 10×10×10 supercell with dimensions of 68.91×68.91×54.03 Å was used for γ-glycine (symmetry group $P3_2$), including 3000 zwitterion molecules and 30000 atoms in total. The particle-mesh Ewald (PME)[45-46] method was used to treat the long-range electrostatic calculations, with a grid spacing of 1 Å; the cut-off values for the Lennard Jones and electrostatic interactions were both set as 12 Å.

Simulations were repeated at different temperatures, with at the temperature the system being initially thermalized using the NPT ensemble. In order to study polarization switching, an external electric field was then applied to the periodic glycine crystals using NVT conditions at 300 K. Do you really mean this … you ran VPT at lots of different temps followed by NVT at 300 K?? why?? The electric field was applied for 2 ns for each trajectory, with the polarization of each system collected after every 1 ps. To maintain constant temperature and pressure, stochastic Langevin dynamics thermostat[47] and Nose–Hoover Langevin piston barostat[48-49] were used, respectively, and the SHAKE algorithm[50] was used for all covalence bonds involving hydrogen atoms. similarly, how was NVT implemented? The NAMD[51] program was employed in all MD simulations.

Results and discussion

First, we performed a series of structural optimizations using different density functionals. The results are summarized in Figure 2. We find that the experimental and optimized structure are in best agreement in terms of lattice constants when using the PBE functional, with a discrepancy less than 2%. The other functionals give a larger discrepancy with respect to the experimental structure about 3% up to 5%, including PBE-D3 at 2.8%. As PBE-D3 includes dispersion effects normally considered to be crucial to the understanding of properties of biological materials, the apparent success of pure PBE indicated that other errors in its treatment of electrostatic interactions compensated for its neglect of the critical dispersion force. While it is unclear how universal this cancellation of errors is likely to be, PBE gives the most realistic results for features of critical relevance to the current work and hence we

continue using it in further studies. Table 1 shows a comparison of PBE-calculated lattice properties with experiment, while details of the PBE electronic structure are given in Supporting Information. This section has to be handled very carefully. Many referees are likely to reject the paper at this point as using a method containing severe errors in regard to the application because of some accidental cancellation like this is usually regarded as being unacceptable – no exceptions. You really have to establish that using PBE wont be disastrous for the main results … there would have been no issue here at all if given Fig 2 you had chosen PBE-D3 for the remaining studies. Really just including PBE and LDA in the list of methods that you used is enough to imply that you don't understand what you are doing and so does not look good.

Table 1. Lattice parameters of glycine from experiments and optimized results from PBE calculation in our work.

Glycine		Lattice parameters						
		a (Å)	b (Å)	c (Å)	∠α (°)	∠β (°)	∠γ (°)	V (Å^3)
EXP	α($P2_1/m$)[13]	5.105	11.972	5.463	90.00	111.74	90.00	310.12
	β($P2_1$)[24]	5.093	6.272	5.385	90.00	113.19	90.00	158.13
	γ($P3_1$)[13]	7.038	7.038	5.481	90.00	90.00	120.00	235.15
	γ($P3_2$)[23]	7.037	7.037	5.481	90.00	90.00	120.00	235.14
OPT	α($P2_1/m$)	5.036	11.602	5.393	90.00	111.82	90.00	292.51
	β($P2_1$)	5.024	6.091	5.317	90.00	113.45	90.00	149.28
	γ($P3_1$)	6.886	6.886	5.408	90.00	90.00	120.00	222.10
	γ($P3_2$)	6.891	6.891	5.403	90.00	90.00	120.00	222.19

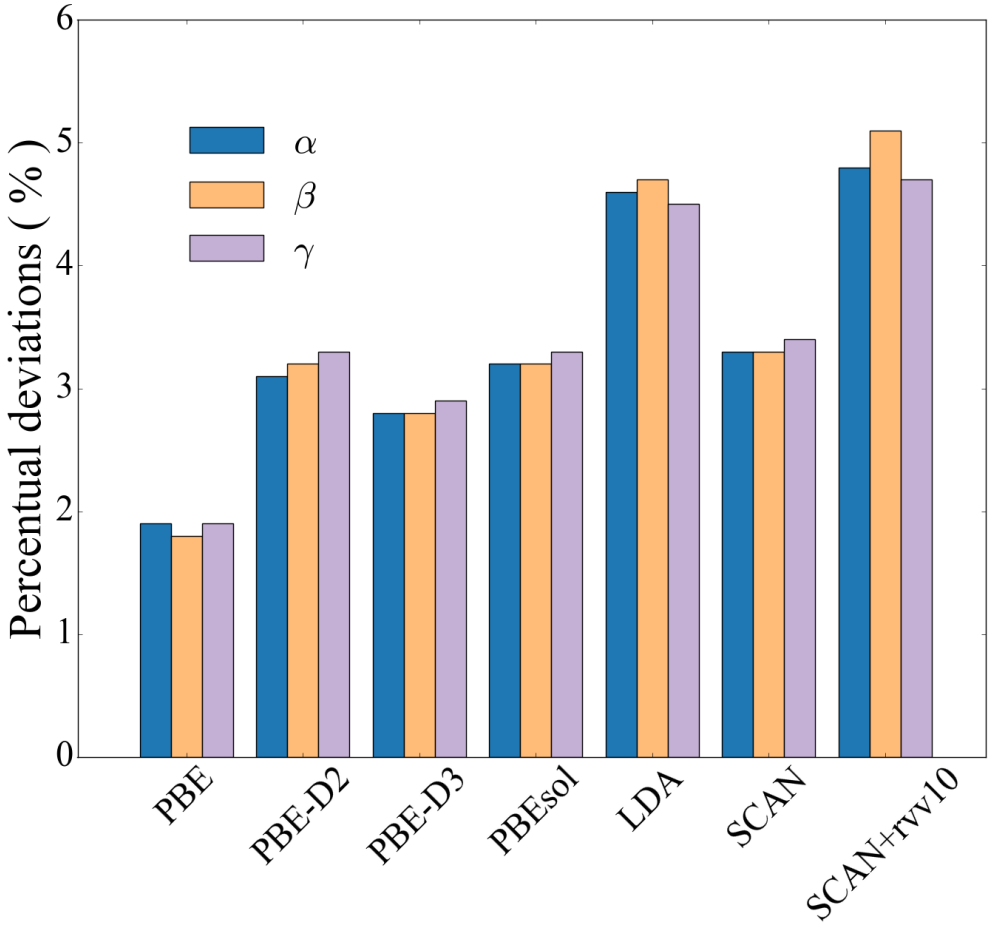

Figure 2. The percentage deviations of lattice constant underestimation after optimization by different functionals. The results of the PBE functional show that the lattice parameter change is less than 2%.

As described in the Methods section, as paraelectric phases corresponding to either β-glycine and γ-glycine are not known, suitable reference structures for the MPT calculations must be artificially constructed. Encompassing the internal structures of glycine crystals, the paths from the observed phases to suitable reference structures are divided into two parts: a pure atomic translation (i.e. displacive distortion field) and a coherent rotation of the molecules (rotational distortion field). We use a fine interpolating mesh of 25 structures along each path.

The total polarization calculated for β-glycine is 11.82 $\mu C/cm^2$ along the b- axis. The smooth curve shown in shown in Figure 3a indicates that the calculation is not affected by polarization quanta. Although the evolution of polarization along the path does not have a real physical meaning and the final value of polarization does not depend on the particular path employed for the calculations[33], useful information can be obtained by a close inspection at the final structural modifications with respect to the paraelectric reference structure. We find that the magnitude of the polarization is strongly affected by the improper dihedral angle between the $-NH_3^+$ group and the plane formed by the carboxyl acid (-COO-). For polarization along the b-axis, the $-NH_3^+$ group undergoes a transition from the paraelectric structure to the ferroelectric one. The molecular dipole moment components along the a-axis and the c-axis cancel out due to symmetry.

Using the same approach, we calculated the polarization of γ-glycine as a function of the dimensionless parameter λ from PE (λ = 0) to FE (λ = 1). The final value is quite large, 70.86 μC/cm² along the c- axis for symmetry $P3_1$ and nearly the same value, 70.66 μC/cm², for symmetry $P3_2$. These values are about five times that for β-glycine (Figure 3a). Along the transition path, the glycine molecules rotate by 180° around an axis perpendicular to the c-axis.

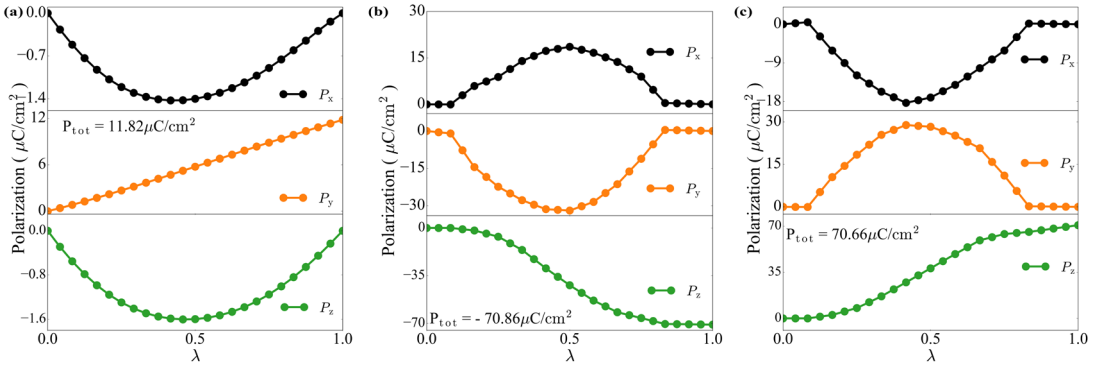

Figure 3. MPT Variation of the polarization of (a) β-glycine, (b) γ-glycine ($P3_1$) and (c) γ-glycine ($P3_2$), along the path between hypothetical paraelectric (λ=0) and observed ferroelectric (λ=1) phases.

To gain more insights into the origin of ferroelectricity in glycine, additional MD simulations were performed, examining the response of the crystal structure and it's polarization to an external electric field at 300 K. Here, we only considered the γ-phase (symmetry group $P3_2$) as the β-phase is extremely unstable and unlikely to be utilized in any application. During the simulation, an external electric field was applied along the c-axis, its strength initially increasing from 0 to 3 V nm^{-1}, then reversed to -3 V nm^{-1}, and then finally returned to 0. The results are shown in Figure 4. Increasing the magnitude of the applied field $|E|$ induced switching form one fully aligned ferroelectric molecular arrangement to another. This switching occurred throughout the range 1 V nm^{-1} < $|E|$ < 2 V nm^{-1}, creating a hysteresis loop. While switching field strengths of this magnitude are large, they are not outside the range achievable in Stark experiments and inside functioning electrical devices. The MD results are consistent with the experimental observation[11] that γ-glycine shows a piezoelectric response at field strengths of 1 V nm^{-1}.

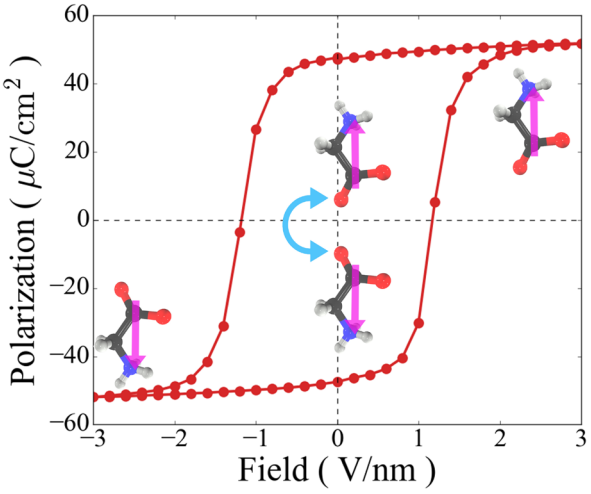

Figure 4. Hysteresis loop showing polarization switching of γ-glycine as controlled by an external applied electric field, at 300 K, obtained from MD simulations. The figure needs V nm^{-1} as its label, E is used as the symbol for field in the text, the unit should be μC cm^{-2}

At the individual molecular level, Figure 5 depicts the spontaneous switching of a γ-glycine crystal from one ferroelectric orientation to the other, at 300 K and constant volume, under a driving electric field of 1.5 V nm^{-1}. Molecules containing molecular dipoles with opposite orientations are displayed in green and red colors respectively, for the domains having polarizations along the +c and −c directions. The sample is first brought to equilibrium using the NVT does not the methods section say NPT ??? ensemble to 300 K until the system was stable, and then we applied an electric field of 1.5 V nm^{-1} for 10 ns to drive polarization switching. Figure 5 shows that product domains begin to nucleate after 0.5 ns, with ferroelectric switching complete after 1.5 ns.

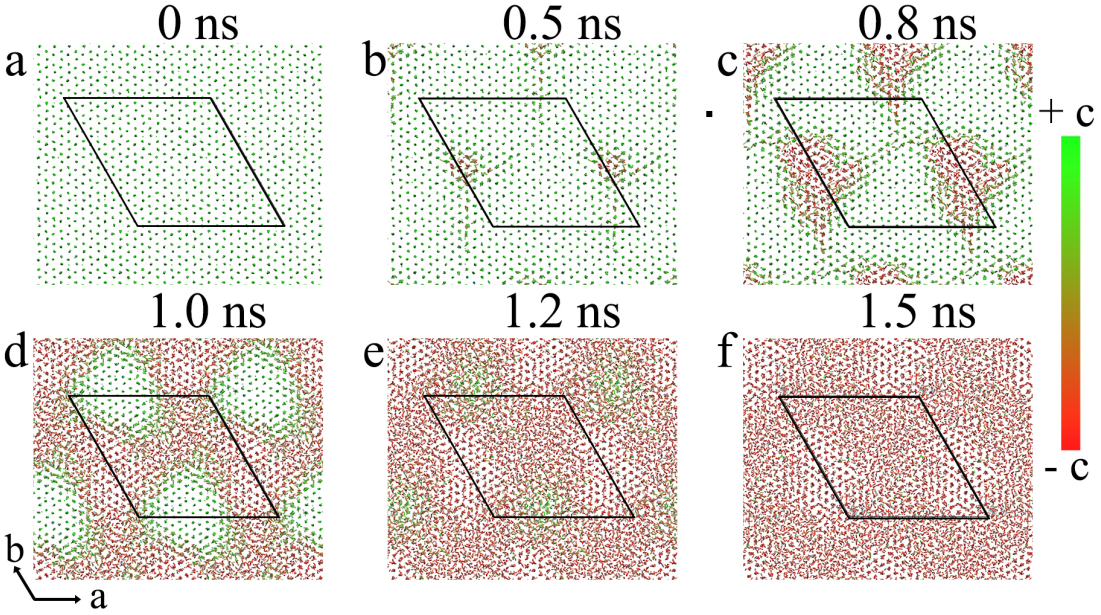

Figure 5. Molecular dynamics simulations of polarization switching when γ-glycine at 300 K experiences an electric field of 1.5 V nm^{-1}. Domain patterns, showing alternatively oriented molecules shaded from red to green, are shown at (a) $t = 0$ ns, (b) $t = 0.5$ ns, (c) $t = 0.8$ ns, (d) $t = 1.0$ ns, (e) $t = 1.2$ ns and (f) $t = 1.5$, revealing that the switching process is completed within approximately 1.5 ns. The font size for the writing in the fig should be 10 or 11 point

Responses to stimuli such as that shown in Figure 6 are usually interpreted in terms of the Kolmogorov-Avrami-Ishibashi (KAI) model.[52-53] This separates the transformation process into two stages: the nucleation of product domains, followed by the growth of these domains. In Fig. 6, these ideas are explored by plotting the fractional conversion from one phase to the other at the different applied field strengths of 1.5 V nm^{-1} (from Figure 5) and 2.0 V nm^{-1}. At both field strengths, different onset times associated with activated nucleation processes are revealed, following by a growth stage that depends quite differently on the applied field, in accordance with model expectations. In more extensive simulations, the physical processes controlling these two responses could be determined. Of particular im-

portance would be how these responses change with changes in external conditions such as temperature, pressure, doping, or chemical substitution, hence defining a required direction for future device research.

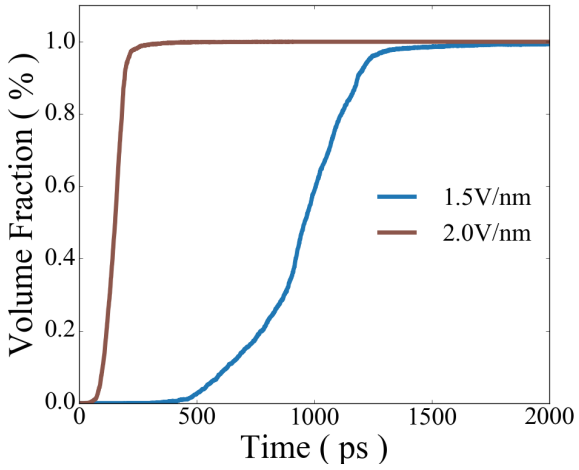

Figure 6. The time-dependent evolution of the growing domain volume fraction during the switching process under electric field strengths of 1.5 V nm (see Fig. 5) and 2.0 V nm. The figure needs V nm^{-1} as its label. Also, ns is discussed in the text not ps, a consistent unit should be used.

Finally, to be useful in some application, ferroelectricity must be maintained over the temperature range of interest. For γ-glycine, MD simulations were performed over the temperature range 100 K to 700 K and the results are shown in Figure 7. As the temperature approaches to 630 K, the average value of the polarization gradually decreases and its fluctuation increases. When the temperature reaches 640 K, the polarization drops sharply to 0.0 μC cm^{-2}, indicating that a ferroelectric phase transition to a paraelectric phase has occurred. The predicted sharp variation of the polarization is suggestive of a first-order phase transition, a result which is profoundly different to that found for the classical ferroelectric material triglycine sulphate (TGS) which instead …… .[54] The calculated order-disorder phase transition temperature of 630 K for γ-gylcene is much higher than the experimentally observed decomposition temperature of the material of about 500 K[reference] below this decomposition temperature, the simulations indicate that glycine will display good ferroelectric properties and hence may be suitable for device applications.

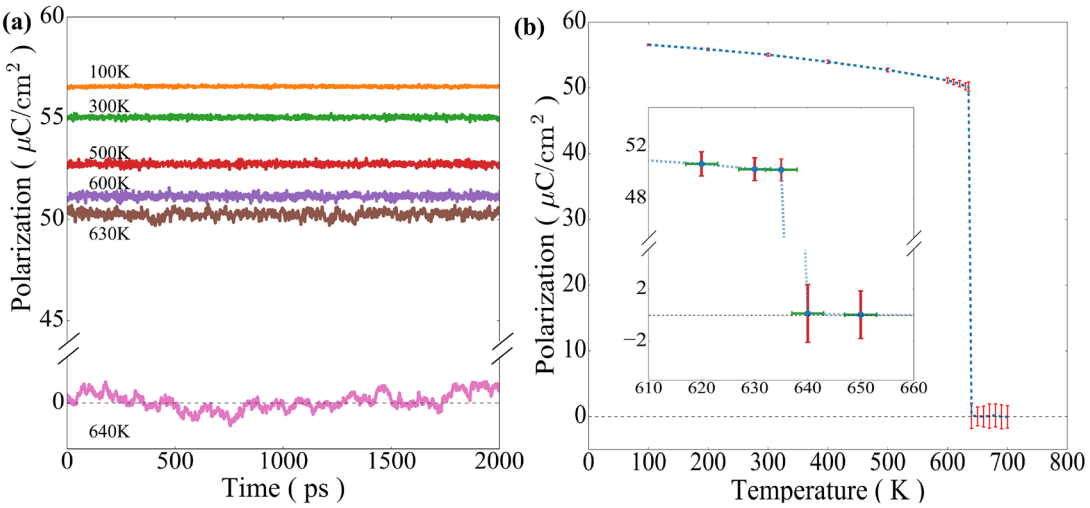

Figure 7. Temperature dependence of polarization of γ-glycine. (a) The polarization profiles from MD simulates below and above the phase transition temperature for 2 ns. (b) Phase transition behavior of γ-glycine and the standard deviation of polarization is indicated by the vertical error bars at each point. Time is given the symbol *t* earlier, units should be ns, space between numbers and units eg "630 K", and the unit should be μC cm^{-2} … getting these things right in the first place always saves a lot of time

Conclusion

In conclusion, we investigated the ferroelectric polarization of β-phase (monoclinic, $P2_1$) and γ-phases (trigonal, $P3_1$ and $P3_2$) of glycine based on first principle calculations and the MPT. Our results predict that γ-glycine should have a spontaneous polarization of 71 μC cm^2 at 300 K. In addition, classical molecular dynamics simulations using PCC charges predict that the polarization of γ-glycine crystals will saturate completely under a sufficiently high extra electric field strength of ca. 1 V nm^{-1}. The order-disorder phase transition is predicted to occur at 630 K, a value higher than the decomposition temperature of glycine. We also indicate that the switching process follows the KAI model, featuring separate timescales for nucleation of the product phase and its subsequent growth. Future studies need to explore the factors controlling each stage to determine how devices will respond to stimuli such as external temperature and pressure changes, doping, and chemical substitution. Given the critical role of glycine in biology, we hope the biocompatibility and ferroelectricity of glycine crystals will make them promising candidates for biomedical applications.

Acknowledgements

This study was funded by the National Nature Science Foundation of China (No. 21503130 to Y.L., and No. 11674212 to Y.L. and J.R.). Y.L. is also supported by the Young Eastern Scholar Program of the Shanghai Municipal Education Commission (QD2016021) and the Shanghai Key Laboratory of High Temperature Superconductors (No. 14DZ2260700). This work was also supported by the National Natural Science Foundation of China (Grants No. 51672171), the National Key Basic Research Program of China (Grant No. 2015CB921600), the Eastern Scholar Program from the Shanghai Municipal Education Commission, and the fund of the State Key Laboratory of Solidification Processing in NWPU (SKLSP201703). Special Program for Applied Research on Super Computation of the NSFC-Guangdong Joint Fund (the second phase), the supercomputing services from AM-HPC, and the Fok Ying Tung Education Foundation are also acknowledged.

References

1. Li, J.; Liu, Y.; Zhang, Y.; Cai, H. L.; Xiong, R. G. Molecular ferroelectrics: where electronics meet biology. *Phys Chem Chem Phys* **2013,** *15* (48), 20786-96.

2. Fukada, E. Piezoelectricity of Wood. *Journal of the Physical Society of Japan* **1955,** *10* (2), 149-154.

3. Liu, Y.; Zhang, Y.; Chow, M. J.; Chen, Q. N.; Li, J. Biological ferroelectricity uncovered in aortic walls by piezoresponse force microscopy. *Phys Rev Lett* **2012,** *108* (7), 078103.

4. Pal, M.; Guo, R.; Bhalla, A. Biological ferroelectricity in human nail samples using Piezoresponse Force Microscopy. *Materials Research Innovations* **2013,** *17* (7), 442-447.

5. Cochran, G. V.; Pawluk, R. J.; Bassett, C. A. Stress generated electric potentials in the mandible and teeth. *Archives of Oral Biology* **1967,** *12* (7), 917,IN25-920,IN25.

6. Li, T.; Zeng, K. Nanoscale piezoelectric and ferroelectric behaviors of seashell by piezoresponse force microscopy. *Journal of Applied Physics* **2013,** *113* (18), 187202.

7. Kholkin, A.; Amdursky, N.; Bdikin, I.; Gazit, E.; Rosenman, G. Strong piezoelectricity in bioinspired peptide nanotubes. *ACS Nano* **2010,** *4* (2), 610-4.

8. Heredia, A.; Bdikin, I.; Kopyl, S.; Mishina, E.; Semin, S.; Sigov, A.; German, K.; Bystrov, V.; Gracio, J.; Kholkin, A. L. Temperature-driven phase transformation in self-assembled diphenylalanine peptide nanotubes. *Journal of Physics D: Applied Physics* **2010,** *43* (46), 462001.

9. Fukada, E.; Yasuda, I. On the Piezoelectric Effect of Bone. *Journal of the Physical Society of Japan* **1957,** *12* (10), 1158-1162.

10. Hu, S.; Jia, F.; Marinescu, C.; Cimpoesu, F.; Qi, Y.; Tao, Y.; Stroppa, A.; Ren, W. Ferroelectric polarization of hydroxyapatite from density functional theory. *RSC Adv.* **2017,** *7* (35), 21375-21379.

11. Heredia, A.; Meunier, V.; Bdikin, I. K.; Gracio, J.; Balke, N.; Jesse, S.; Tselev, A.; Agarwal, P. K.; Sumpter, B. G.; Kalinin, S. V.; Kholkin, A. L. Nanoscale Ferroelectricity in Crystalline γ-Glycine. *Advanced Functional Materials* **2012,** *22* (14), 2996-3003.

12. Elsila, J. E.; Dworkin, J. P.; Bernstein, M. P.; Martin, M. P.; Sandford, S. A. Mechanisms of Amino Acid Formation in Interstellar Ice Analogs. *Astrophysical Journal* **2007,** *660* (1), 911.

13. Boldyreva, E. V.; Drebushchak, T. N.; Shutova, E. S. Structural distortion of the α, β, and γ

polymorphs of glycine on cooling. *Zeitschrift für Kristallographie - Crystalline Materials* **2003,** *218* (5).
14. Albrecht, G.; Corey, R. B. The Crystal Structure of Glycine. *Journal of the American Chemical Society* **1939,** *61* (5), 1087-1103.
15. Dawson, A.; Allan, D. R.; Belmonte, S. A.; Clark, S. J.; David, W. I. F.; McGregor, P. A.; Parsons, S.; Pulham, C. R.; Sawyer, L. Effect of High Pressure on the Crystal Structures of Polymorphs of Glycine. *Crystal Growth & Design* **2005,** *5* (4), 1415-1427.
16. Goryainov, S. V.; Boldyreva, E. V.; Kolesnik, E. N. Raman observation of a new (ζ) polymorph of glycine? *Chemical Physics Letters* **2006,** *419* (4), 496-500.
17. Iitaka, Y. Crystal Structure of β-Glycine. *Nature* **1959,** *183* (4658), 390-391.
18. Iitaka, Y. The crystal structure of γ-glycine. *Acta Crystallographica* **1961,** *14* (1), 1-10.
19. Perlovich, G. L.; Hansen, L. K.; Bauer-Brandl, A. The Polymorphism of Glycine. Thermochemical and structural aspects. *Journal of Thermal Analysis and Calorimetry* **2001,** *66* (3), 699-715.
20. Park, K.; Evans, J. M. B.; Myerson, A. S. Determination of Solubility of Polymorphs Using Differential Scanning Calorimetry. *Crystal Growth & Design* **2003,** *3* (6), 991-995.
21. Bystrov, V. S.; Seyedhosseini, E.; Bdikin, I.; Kopyl, S.; Neumayer, S. M.; Coutinho, J.; Kholkin, A. L. Bioferroelectricity in Nanostructured Glycine and Thymine: Molecular Modeling and Ferroelectric Properties at the Nanoscale. *Ferroelectrics* **2015,** *475* (1), 107-126.
22. Resta, R.; Vanderbilt, D. Theory of Polarization: A Modern Approach. *Topics in Applied Physics* **2007,** *105*, 31-68.
23. Latajka, Z.; Ratajczak, H. Molecular orbital calculations for glycine crystals. *The Journal of Physical Chemistry* **1979,** *83* (21), 2785-2787.
24. Drebushchak, T. y. N.; Boldyreva, E. V.; Shutova, E. S. β-Glycine. *Acta Crystallographica* **2002,** *58* (6), o634-o636.
25. Centre, C. C. D. Cambridge_Crystallographic_Data_Centre. *Crystallography*.
26. Kresse, G.; Furthmüller, J. Efficient iterative schemes for ab initio total-energy calculations using a plane-wave basis set. *Physical Review B* **1996,** *54* (16), 11169-11186.
27. Kresse, G.; Joubert, D. From ultrasoft pseudopotentials to the projector augmented-wave method. *Physical Review B* **1999,** *59* (3), 1758-1775.
28. Perdew, J. P.; Burke, K.; Ernzerhof, M. Generalized Gradient Approximation Made Simple. *Physical Review Letters* **1996,** *77* (18), 3865-3868.
29. Perdew, J. P.; Wang, Y. Accurate and simple analytic representation of the electron-gas correlation energy. *Physical Review B Condensed Matter* **1992,** *45* (23), 13244.
30. Grimme, S.; Antony, J.; Ehrlich, S.; Krieg, H. A consistent and accurate ab initio parametrization of density functional dispersion correction (DFT-D) for the 94 elements H-Pu. *Journal of Chemical Physics* **2010,** *132* (15), 154104.
31. Grimme, S. Semiempirical GGA‐type density functional constructed with a long‐range dispersion correction. *Journal of Computational Chemistry* **2006,** *27* (15), 1787-99.
32. Perdew, J. P.; Ruzsinszky, A.; Csonka, G. I.; Vydrov, O. A.; Scuseria, G. E.; Constantin, L. A.; Zhou, X.; Burke, K. Restoring the Density-Gradient Expansion for Exchange in Solids and Surfaces. *Physical Review Letters* **2008,** *100* (13), 136406.
33. Sun, J.; Ruzsinszky, A.; Perdew, J. P. Strongly Constrained and Appropriately Normed Semilocal Density Functional. *Physical Review Letters* **2015,** *115* (3), 036402.
34. Peng, H.; Yang, Z.-H.; Perdew, J. P.; Sun, J. Versatile van der Waals Density Functional Based on a

Meta-Generalized Gradient Approximation. *Physical Review X* **2016,** *6* (4).
35. Momma, K.; Izumi, F. VESTA 3 for three-dimensional visualization of crystal, volumetric and morphology data. *Journal of Applied Crystallography* **2011,** *44* (6), 1272-1276.
36. Resta, R. Macroscopic polarization in crystalline dielectrics: the geometric phase approach. *Reviews of Modern Physics* **1994,** *66* (3), 899-915.
37. King-Smith, R. D.; Vanderbilt, D. Theory of polarization of crystalline solids. *Physical Review B Condensed Matter* **1993,** *47* (3), 1651.
38. Hu, S.; Gao, H.; Qi, Y.; Tao, Y.; Li, Y.; Reimers, J. R.; Bokdam, M.; Franchini, C.; Di Sante, D.; Stroppa, A.; Ren, W. Dipole Order in Halide Perovskites: Polarization and Rashba Band Splittings. *The Journal of Physical Chemistry C* **2017,** *121* (41), 23045-23054.
39. Capillas, C.; Tasci, E. S.; Gemma, D. L. F.; Orobengoa, D.; Perezmato, J. M.; Aroyo, M. I. A new computer tool at the Bilbao Crystallographic Server to detect and characterize pseudosymmetry. *Crystalline Materials* **2011,** *226* (2), 186-196.
40. Perezmato, J. M.; Orobengoa, D.; Aroyo, M. I. Mode crystallography of distorted structures. *Acta Crystallographica Section A Foundations of Crystallography* **2010,** *66* (5), 558.
41. Orobengoa, D.; Capillas, C.; Aroyo, M. I.; Perez-Mato, J. M. AMPLIMODES : symmetry-mode analysis on the Bilbao Crystallographic Server. *Journal of Applied Crystallography* **2010,** *42* (5), 820-833.
42. Case, D. A.; Iii, T. E. C.; Darden, T.; Gohlke, H.; Luo, R.; Jr, K. M. M.; Onufriev, A.; Simmerling, C.; Wang, B.; Woods, R. J. The Amber Biomolecular Simulation Programs. *Journal of Computational Chemistry* **2005,** *26* (16), 1668-88.
43. Li, Y. L.; Mei, Y.; Zhang, D. W.; Xie, D. Q.; Zhang, J. Z. H. Structure and Dynamics of a Dizinc Metalloprotein: Effect of Charge Transfer and Polarization. *Journal of Physical Chemistry B* **2011,** *115* (33), 10154-10162.
44. Tong, Y.; Mei, Y.; Li, Y. L.; Ji, C. G.; Zhang, J. Z. H. Electrostatic Polarization Makes a Substantial Contribution to the Free Energy of Avidin−Biotin Binding. *Journal of the American Chemical Society* **2010,** *132* (14), 5137-5142.
45. Darden, T.; York, D.; Pedersen, L. Particle mesh Ewald: An N·log(N) method for Ewald sums in large systems. *Journal of Chemical Physics* **1998,** *98* (12), 10089-10092.
46. Essmann, U. A smooth particle mesh Ewald method. *Journal of Chemical Physics* **1995,** *103* (19), 8577-8593.
47. Pastor, R.; Brooks, B.; AttilaSzabo. An analysis of the accuracy of Langevin and molecular dynamics algorithms. *Molecular Physics* **2006,** *65* (6), 1409-1419.
48. Martyna, G. J.; Tobias, D. J.; Klein, M. L. Constant pressure molecular dynamics algorithms. *Journal of Chemical Physics* **1994,** *101* (5), 4177-4189.
49. Feller, S. E.; Zhang, Y.; Pastor, R. W.; Brooks, B. R. Constant pressure molecular dynamics simulation: The Langevin piston method. *Journal of Chemical Physics* **1998,** *103* (11), 4613-4621.
50. Ryckaert, J. P.; Ciccotti, G.; Berendsen, H. J. C. Numerical integration of the cartesian equations of motion of a system with constraints: molecular dynamics of n-alkanes. *Journal of Computational Physics* **1977,** *23* (3), 327-341.
51. Phillips, J. C.; Braun, R.; Wang, W.; Gumbart, J.; Tajkhorshid, E.; Villa, E.; Chipot, C.; Skeel, R. D.; Kalé, L.; Schulten, K. Scalable Molecular Dynamics with NAMD. *Journal of Computational Chemistry* **2005,** *26* (16), 1781-802.
52. Jo, J. Y.; Han, H. S.; Yoon, J. G.; Song, T. K.; Kim, S. H.; Noh, T. W. Domain Switching Kinetics in

Disordered Ferroelectric Thin Films. *Physical Review Letters* **2007,** *99* (26), 267602.
53. Boddu, V.; Endres, F.; Steinmann, P. Molecular dynamics study of ferroelectric domain nucleation and domain switching dynamics. *Sci Rep* **2017,** *7* (1), 806.
54. Matthias, B. T.; Miller, C. E.; Remeika, J. P. Ferroelectricity of Glycine Sulfate. *Physical Review* **1956,** *104* (3), 849-850.